Contents lists available at GrowingScience

Current Chemistry Letters

homepage: www.GrowingScience.com

Exploring the impact of spacers in novel indole-based D–π–D–A dyes for high-efficiency DSSCs: A DFT/TD-DFT study

Mohamed Reda Chriyaa[a], Hayat EL Ouafy[a], Walid Iken[a], Soukaina Naciri[a], Mouad Boutkbout Nait Moudou[a], Mouna Aamor[a], Loubna Halil[a] and Tarik EL Ouafy[b*]

[a]*Laboratory of Engineering in Chemistry and Physics of Matter, Faculty of Sciences and Technics, Sultan Moulay Slimane University, Beni Mellal, Morocco*
[b]*Laboratory of Engineering in Chemistry and Physics of Matter, Faculty of Medicine and Pharmacy, Sultan Moulay Slimane University, Beni Mellal, Morocco*

C H R O N I C L E

Article history:
Received October 16, 2024
Received in revised form
November 2, 2024
Accepted March 19, 2025
Available online
March 19, 2025

Keywords:
DSSCs
π-bridge
DFT studies
Charge transfer
B3LYP

A B S T R A C T

Population growth and economic development have led to an increase in global energy consumption. Solar energy, a major renewable source, is essential to meeting human energy needs. This study, four new organic dyes (A_1–A_4) with a D–π–D–A structure using DFT and TD-DFT techniques for their potential application in dye-sensitized solar cells (DSSCs). The impact of π-bridge modifications of the A_0 (reference molecule) on the structural, photovoltaic, optical and electronic properties was analyzed. The dyes showed band gaps (Egap) ranging from 2.4 to 3.5eV and absorption wavelengths (λ) from 420.16 to 627.4nm. Results suggest that the modification of the π-bridge of dye A_0 enhanced intramolecular charge transfer (ICT). and improved hole injection. Theoretical open-circuit voltages (Voc) varied between 1.15 and 2.36 eV, while light harvesting efficiency (LHE) values ranged from 0.80 to 0.93. This study could effectively assist chemists in the synthesis of efficient dyes for DSSCs.

1. Introduction

In the current context, the use of energy plays a crucial role in human life, and the demand for available resources continues to grow. Solar energy, being a renewable, clean, and eco-friendly resource, is increasingly considered a viable alternative to traditional resources.

One of the most important challenges of this century is to enhance the efficiency of converting solar photons into electricity. For solar energy to play an important role in carbon-free energy supply, it must be economically competitive with nuclear energy, fossil fuels, and other renewable energy sources. This requires significant advances in both fundamental research and applied sciences to reduce the costs of solar energy production.[1]
Among the various renewable energy sources, DSSCs stand out as a promising alternative to traditional silicon-based solar cells.

DSSCs, also known as photoelectrochemical solar cells, utilize a photo-induced reaction on a semiconductor electrode within a modified electrochemical cell. They offer numerous advantages, including reduced manufacturing costs, simplicity of production, and efficient performance under various ambient conditions. Additionally, they are environmentally friendly, both indoors and outdoors.[2,3]

The structure of DSSCs generally consists of a sandwich-like arrangement comprising a working electrode, a counter electrode and an electrolyte. Under sunlight illumination, dye molecules are excited by photon absorption, leading to the injection of excited electrons into the conduction band of the semiconductor surface (photoanode). Subsequently, these

* Corresponding author
E-mail address tarikelouafy@gamil.com (T. EL Ouafy)

doi: 10.5267/j.ccl.2025.3.004

electrons are transferred to the counter electrode via the external circuit, while redox reactions occur in the mediator electrolyte containing the redox couple R/R^+. Through these redox reactions, electrons are transferred back to the oxidized dye molecules, returning the oxidized dye to its original state, with these processes occurring cyclically.[4,5]

The overall performance of DSSCs primarily depends on the number of photons absorbed by the dye molecules. Light-harvesting sensitizers play a crucial role in inducing the photocurrent, due to their low energy gap and appropriate energy level for electron injection. However, metal complex dyes present issues of cost and availability, limiting their commercial application. In contrast, metal-free organic photosensitizers are garnering increasing interest and have achieved a maximum power conversion efficiency (PCE) of 14% with the use of co-sensitizers.[6,7] The design of DSSCs relies on the use of photosensitive materials in solar cells; typically, a DSSC consists of four primary components: the sensitizer, the electrolyte, the cathode and the anode.[8] The anode in DSSCs is made up of a thin layer of nanocrystalline metal oxide, such as titanium dioxide (TiO_2) or zinc oxide (ZnO), which is deposited onto a glass substrate.[9] Sensitizers, whether natural or synthetic, are crucial components of DSSCs, playing a key role in expanding their absorption spectrum.[10] In this regard, various organometallic, natural and organic dyes can be used as sensitizers.[11] The electrolyte in a DSSC is composed of a redox couple, typically iodide/triiodide (I^-/I^{3-}), enclosed by a counter electrode, which is usually made of platinum.[12]
Most organic dyes used in DSSCs typically feature a D–π–A (donor–π-bridge–acceptor) molecular structure, which is engineered to facilitate intramolecular charge transport (ICT) from the donor unit (D) towards the acceptor group (A) through the π-bridge.[13,14] Additionally, other sensitizer structures such as A–π–D–π–A, D–π–D–A, D–D–π–A and D–A–π–A have been developed and have gained significant attention for their high efficiency.[15,16]

The choice of the π-bridge is critical in the design of D–π–A dyes, as it significantly influences the regulation of HOMO–LUMO energy levels and broadens the absorption range of organic sensitizers. In this work, we developed a series of organic dyes (A_1–A_4) with the D–π–D–A system as sensitizers. Among these sensitizers, DPC (referred to as A0 in this paper) exhibited a performance of 1.22%. (Jsc = 4.41 mA cm^{-2}, FF = 0.56 and Voc = 0.522 V),[17] using carboxylic acid as the electron acceptor and benzene as the π-bridge (**Fig. 1**).

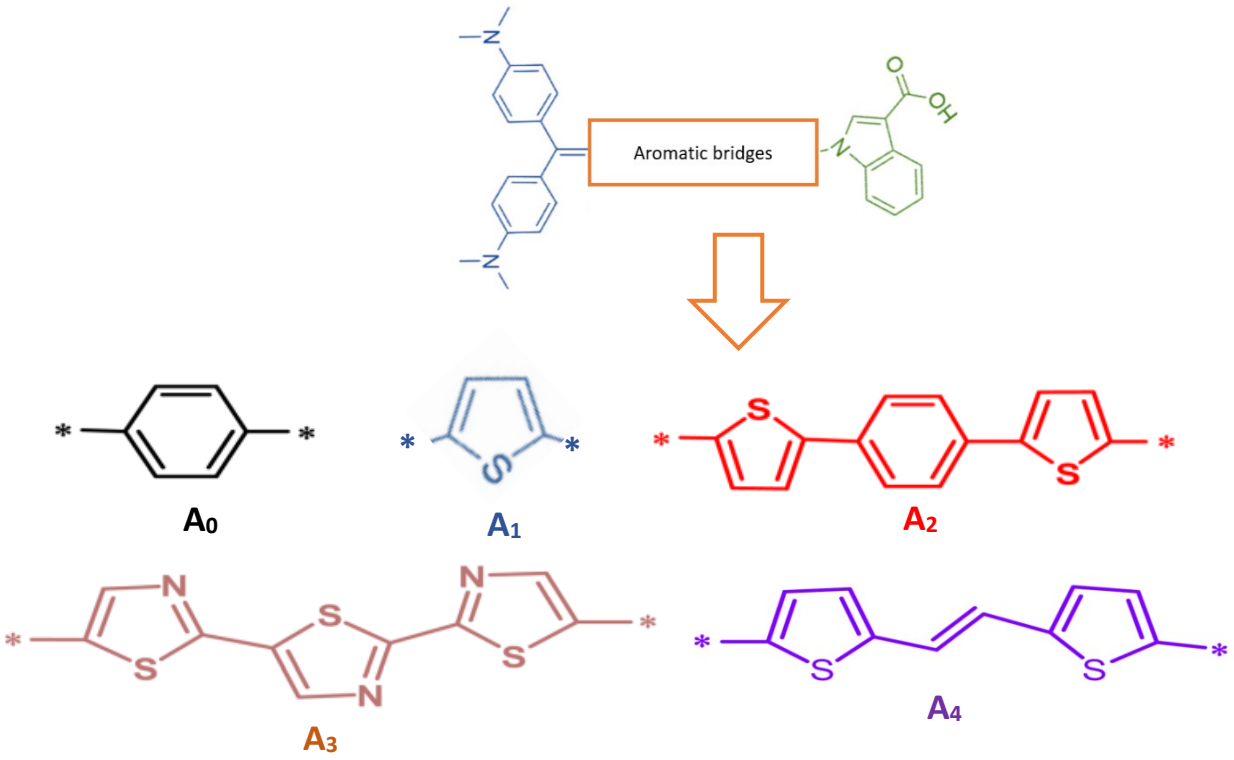

Fig. 1. Chemical structure of studied dyes (A_0–A_4)

The π-bridge plays a crucial role in facilitating the swift transfer of electrons for charging DSSCs; therefore, it must possess the following characteristics: easy charge transport, an extended π-bridge that covers a broad portion of the light absorption spectrum, and enhanced absorption capability.[18] Thus, choosing an appropriate π-bridge is a crucial step in constructing high-performance photovoltaic cells. Various π-bridges have been theoretically explored to develop new sensitizers, utilizing DFT and TD-DFT methods to elucidate the effects of different π-bridge compounds (A_1–A_4). By identifying the critical theoretical elements, a high current charge density (Jsc), open-circuit voltage (Voc), light-harvesting efficiency (LHE), electron injection driving force (ΔG^{inject}), and driving force of regeneration (ΔG_{reg}) were determined. Additionally, other factors like energy levels, density of states (DOS), frontier molecular orbitals (FMOs), chemical indices, and absorption spectra were also taken into account. These theoretical parameters assist in clarifying the link between molecular structure and performance, aiding in the selection of better dyes.[20] Additional parameters, including frontier

molecular orbitals (FMOs), energy levels, density of states (DOS), absorption spectra, and chemical indices, were also analyzed. These theoretical parameters aid in clarifying the connection between performance and molecular structure, aiding in the selection of better dyes.[19]

2. Calculation section

Numerous computational parameters can impact the performance of dye-sensitized solar cells (DSSCs), particularly affecting the power conversion efficiency (η). This efficiency is determined by several factors, including the values of Jsc, Voc, the the incident solar power (Pinc) and fill factor (FF).[16]

$$\eta = \frac{\text{Voc} \,.\, \text{Jsc} \,.\, \text{FF}}{\text{Pinc}}$$

The Voc parameter can be determined using the following analytical relationship:

$$\text{Voc} = E_{LUMO} - E_{CB}$$

where E_{LUMO} represents the energy level of the dye, and E_{CB} corresponds to the conduction band energy of TiO_2 (E_{CB} = −4,0 eV).[21] In a DSSC, Jsc can be calculated using the following equation:

$$\text{Jsc} = \int \text{LHE}\,(\lambda) \,.\, \varphi_{inject} \,.\, \eta_{collect}\, d\,\lambda$$

where LHE(λ) represents the light-harvesting efficiency at a particular wavelength, η stands for the charge collection efficiency and φ_{inject} denotes the electron injection efficiency.[22] It is crucial to note that the LHE of DSSCs is a key factor affecting their performance. Generally, a high LHE results in a greater amount of photocurrent. The LHE can be calculated using the following equation:

$$\text{LHE} = 1 - 10^{-f}$$

where *f* represents the oscillator strength relative to the λ_{max} of the dye. This strength directly influences the LHE. The following equation can be utilized to determine the injection force into the TiO_2 conduction band.[23]

$$\Delta G^{inject} = E^{dye*} - E_{CB}$$

In this context, E^{dye*} denotes the oxidation potential of the dye in its excited state, while E_{CB} denotes the reduction potential of the conduction band (TiO_2 = − 4.0 eV).[24] The value of E^{dye*} can be determined using the following equation:

$$E^{dye*} = E^{dye} - E^{00}$$

E^{dye} represents the oxidation potential of the molecule in its neutral state ($E^{dye} = -E_{HOMO}$), and E^{00} corresponds to the vertical transition energy to λ_{max} .

To ensure swift electron transfer, ΔG_{reg} needs to be minimized. The driving force for the regeneration of the dye, noted as ΔG_{reg}, is calculated as follows:

$$\Delta G_{reg} = E^{dye} - E_{\text{Redox}}^{\text{Electrolyte}}$$

where $E_{\text{Redox}}^{\text{Electrolyte}}$ is the redox potential of the I^-/I^{3-} electrolyte (−4.80 eV).[25,27] Using the energy levels of the frontier molecular orbitals (HOMO and LUMO), the chemical potential (μ), electronegativity (χ), and chemical hardness (η) can be calculated according to the following formulas: [26,28]

$$\mu = \frac{E_{LUMO} + E_{HOMO}}{2}$$

$$\chi = -\mu = -\frac{E_{LUMO} + E_{HOMO}}{2}$$

$$\eta = \frac{E_{LUMO} - E_{HOMO}}{2}$$

3. Validation of the Calculation Method

The calculations in this study were executed with the Gaussian 09 software package, and GaussView 6.0.16 was employed for generating the simulated spectra and analyzing orbital density. The selection of the TD-DFT theoretical functional for describing the vertical transition energy of a potential sensitizer is determined by the λ_{max} (absorption wavelengths) of the reference molecule.

Fig. 2 displays the λmax of the reference molecule, analyzed using TD-DFT with different functionals, including CAM-B3LYP, PBEPBE, MPW1PW91, and B3LYP, [29,31] in combination with the 6-311G basis set. The B3LYP functional with the 6-311G basis set accurately calculated the maximum absorption wavelength (λmax) of the compound at 381 nm, which is in close agreement with the experimentally observed value of 383 nm. [17]These results reinforce the reliability of B3LYP in predicting electronic transitions in π-conjugated systems, making it an appropriate method for studying light absorption in DSSCs. Moreover, several studies have confirmed that B3LYP/6-311G provides optimal accuracy for predicting absorption wavelengths in DSSCs, further supporting its suitability for studying organic dyes.[20,32] This computational accuracy led to the selection of B3LYP/6-311G for further investigations into the optical properties of the four proposed molecules (A_1, A_2, A_3, and A_4).

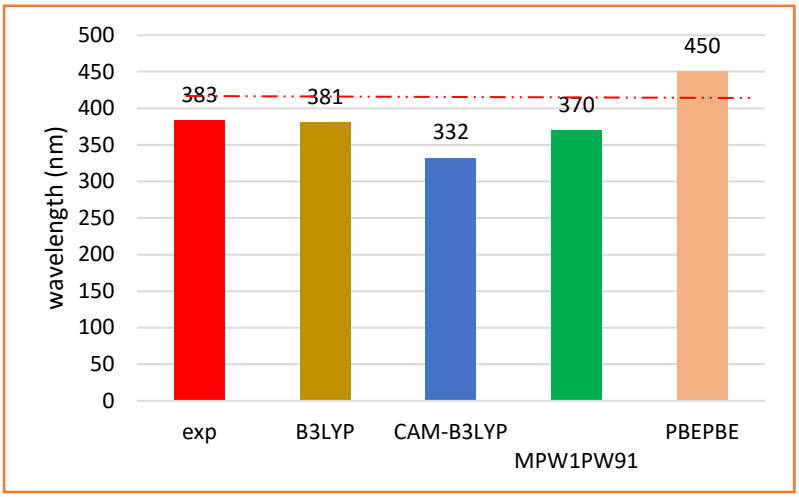

Fig. 2. Analyzing the functional employed in the TD-DFT calculation for determining the maximum absorption wavelengths (λmax) for A_0

4. Results and discussion

4.1 Synthesis of dyes

The synthesis of A_0 (1-(4-(2,2-bis(4-(dimethylamino)phenyl)vinyl)phenyl)-1H-indole-3-carboxylic acid) follows a multi-step approach involving Wittig olefination and Ullmann coupling, which are well-established methods for constructing π-conjugated organic molecules. These reactions facilitate the development of electron-rich and highly conjugated systems, crucial for applications in organic photovoltaics and dye-sensitized solar cells (DSSCs).[30]

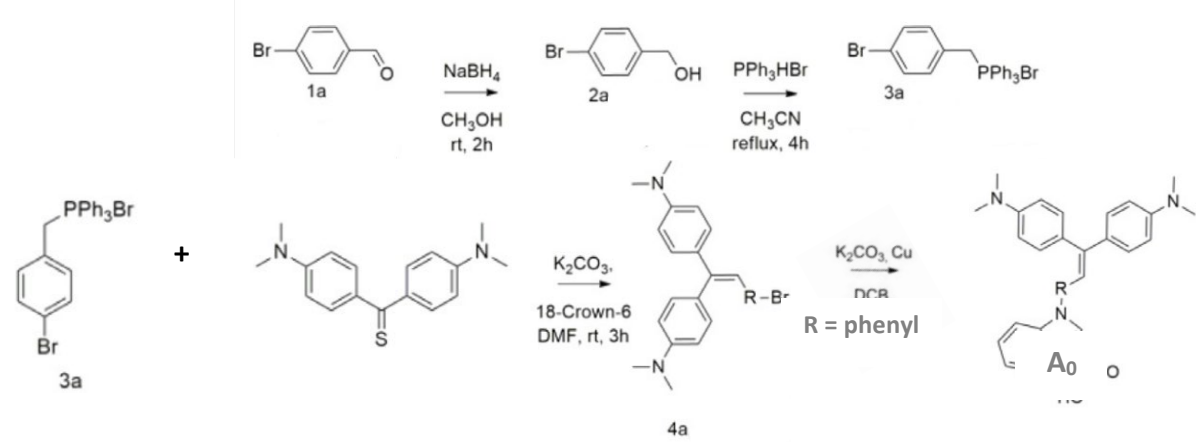

Fig. 3. Synthetic route to synthesize organic dyes A_0

The first step in the synthesis involves the preparation of phosphonium intermediates (3a). This process begins with the 4-bromobenzaldehyde (1a), which undergo transformation into phosphonium salts (3a) via primary alcohol intermediates (2a). The introduction of these phosphonium salts is a key step, as they serve as essential precursors in the subsequent Wittig olefination reaction.[17]

The next step is the Wittig olefination reaction, where the phosphonium salts (3a) react with 4,4′-bis(dimethylamino)thiobenzophenone in the presence of K_2CO_3 as a base. This reaction leads to the formation of the highly

conjugated intermediates (4a), which play a crucial role in optimizing the electronic properties of the final product. The use of Wittig olefination in organic dye synthesis has been widely applied due to its efficiency in forming extended π-systems with tailored electronic properties.[17] The final step involves the Ullmann coupling reaction, where the intermediate (4a) is coupled with 1H-indole-3-carboxylic acid in the presence of K_2CO_3. The Ullmann reaction is a widely utilized method for C-C and C-N bond formation in organic synthesis, particularly for the construction of donor-acceptor (D–A) molecular frameworks used in DSSCs. This step leads to the formation of A_0, a indole-based dye with enhanced charge-transfer properties.

4.2 Molecular Geometry

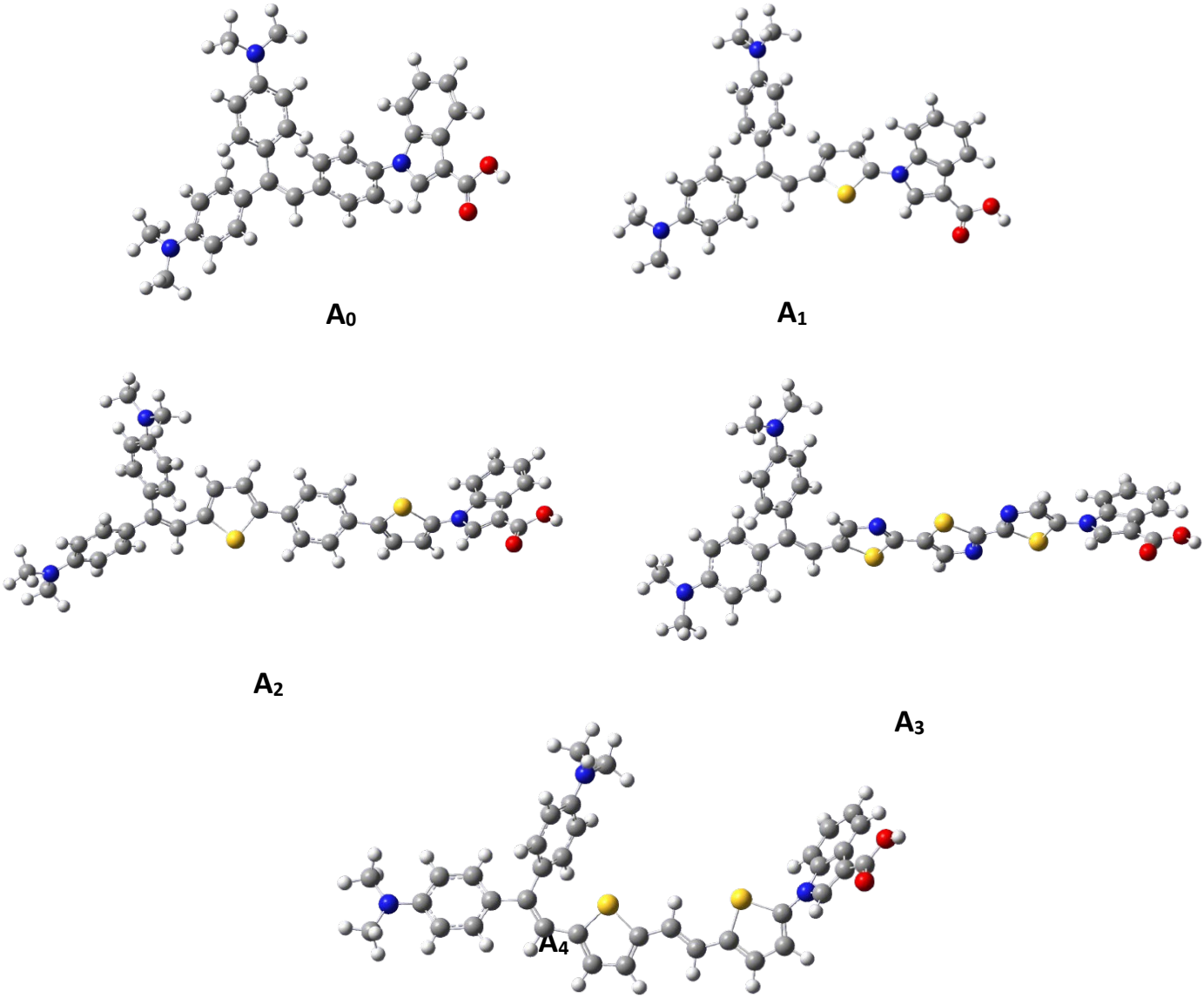

Fig.. 4 Optimized structures of all the compounds studied obtained by B3LYP/6-31G.

The geometric properties of the potential sensitizer structures are shown in Table 1, where d represents the bond lengths (**Scheme 1**). All parameters were calculated at the DFT/B3LYP/6-31G level, which is a well-established method for predicting accurate molecular geometries in DSSCs. B3LYP has been widely validated for its ability to provide reliable bond lengths and angles in π-conjugated systems, ensuring consistency with experimental data. [30,33] The 6-31G basis set offers a computationally efficient approach while maintaining sufficient accuracy for structural optimizations. Studies have confirmed that B3LYP/6-31G yields molecular geometries in good agreement with crystallographic and spectroscopic data, making it a suitable choice for this study.[30,33]

Notably, shorter bond lengths are advantageous for intramolecular charge transport within the D–π–D–A architecture .[34] The optimized structures of all the studied dyes show similar conformations, as confirmed by the bond length values ranging between 1.40 and 1.46 Å. These bond lengths suggest a C=C character in all the dyes, thus facilitating charge transport between the donor fragment and the π-bridge, and also between the π-bridge and the acceptor fragment.[35]

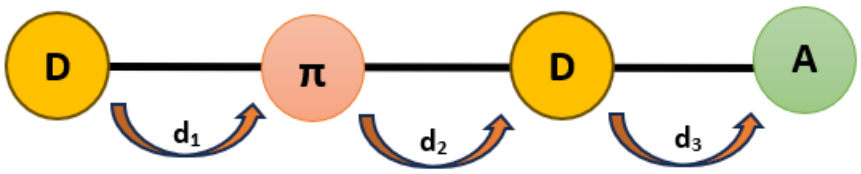

Scheme 1. bond lengths (d_1, d_2, d_3, in Å)

Table. 1. Selected bond lengths (in Å) of the designed structures

dye	d_1 (Å)	d_2 (Å)	d_3 (Å)
A_0	1.46	1.43	1.45
A_1	1.45	1.41	1.45
A_2	1.44	1.41	1.45
A_3	1.44	1.40	1.44
A_4	1.43	1.40	1.44

4.2 Frontier Molecular Orbitals

The frontier molecular orbitals (HOMO and LUMO) act as quantum descriptors, offering vital insights into the optoelectronic properties of the dyes. They enable the examination of charge density distribution and stabilization within the dyes.[35,36] According to the literature, electron transfer ($S_0 \rightarrow S_1$) in each observed dye occurs as electrons move from the ground state (HOMO) to LUMO (the excited state).[37] The HOMO-LUMO gap (Eg) reflects the variations in reactivity due to different π-spacers. A smaller band gap facilitates charge transfer, while a larger gap makes it more difficult.[35]

Determining the theoretical energy levels of the HOMO and LUMO for each dye is essential for comprehending the electronic properties of dye systems.[38,35] This evaluation helps to assess whether the proposed dyes meet the fundamental requirements of photosensitizer materials for DSSCs. The values of E_{HOMO}, E_{LUMO}, as well as the different E_{gap} values for the studied molecules, are presented in **Fig. 5**, while the schematic of the frontier molecular orbitals is illustrated in **Table 2**.

The analysis of the frontier orbitals showed that for the studied dyes A_0, A_1, A_2, A_3, and A_4, the HOMO electrons were concentrated on the donor, with a few of them distributed near the bridge. At the same time, the LUMO was widely distributed across these dyes, with maximum density on various π-spacers and minimal density on the acceptor groups. This distribution indicates that charge transfer occurs efficiently from the donor to the π-spacers, thereby facilitating light absorption and electron injection in DSSC devices.

In particular, the high concentration of electronic density on the π-spacers suggests an enhanced capacity of these molecules to transfer excited electrons to the acceptor groups, thereby optimizing the efficiency of converting solar energy into electrical energy in DSSCs.

The energy levels of molecules A_0 to A_4 were calculated using the B3LYP/6-311G+(d,p) method.

Studies have demonstrated that B3LYP reliably predicts HOMO-LUMO energy levels with minimal deviation from experimental data, ensuring its suitability for investigating charge transfer in DSSCs. Additionally, the 6-311G+(d,p) basis set enhances accuracy by incorporating both diffuse and polarization functions, which are crucial for modeling intramolecular charge transfer. [39,40] These factors establish B3LYP/6-311G+(d,p) as an optimal choice for studying the electronic properties of the designed photosensitizers.

The results in **Table 2** indicate that the HOMO levels of all the molecules were lower than the redox potential of the I^-/I^{3-} couple. As a result, the photosensitizers are capable of being reduced by electrons from the I^-/I^{3-} electrolyte.

Additionally, the molecules displayed LUMO values exceeding the conduction band of TiO_2 (−4.00 eV), suggesting that electrons can be swiftly injected into the TiO_2 semiconductor when the molecules are excited. Thus, the proposed dyes (A_0 to A_4) are good candidates as photosensitizers and are well-suited for applications in DSSCs.[41]

The energy gap plays a crucial role in the activity of molecules; a sensitizer with a lower bandgap energy is more favorable to electron excitation and demonstrates improved absorption properties. As a result, such sensitizers can absorb more photons in the visible spectrum, leading to an increase in short-circuit current (Jsc) and power conversion efficiency (PCE).[42]

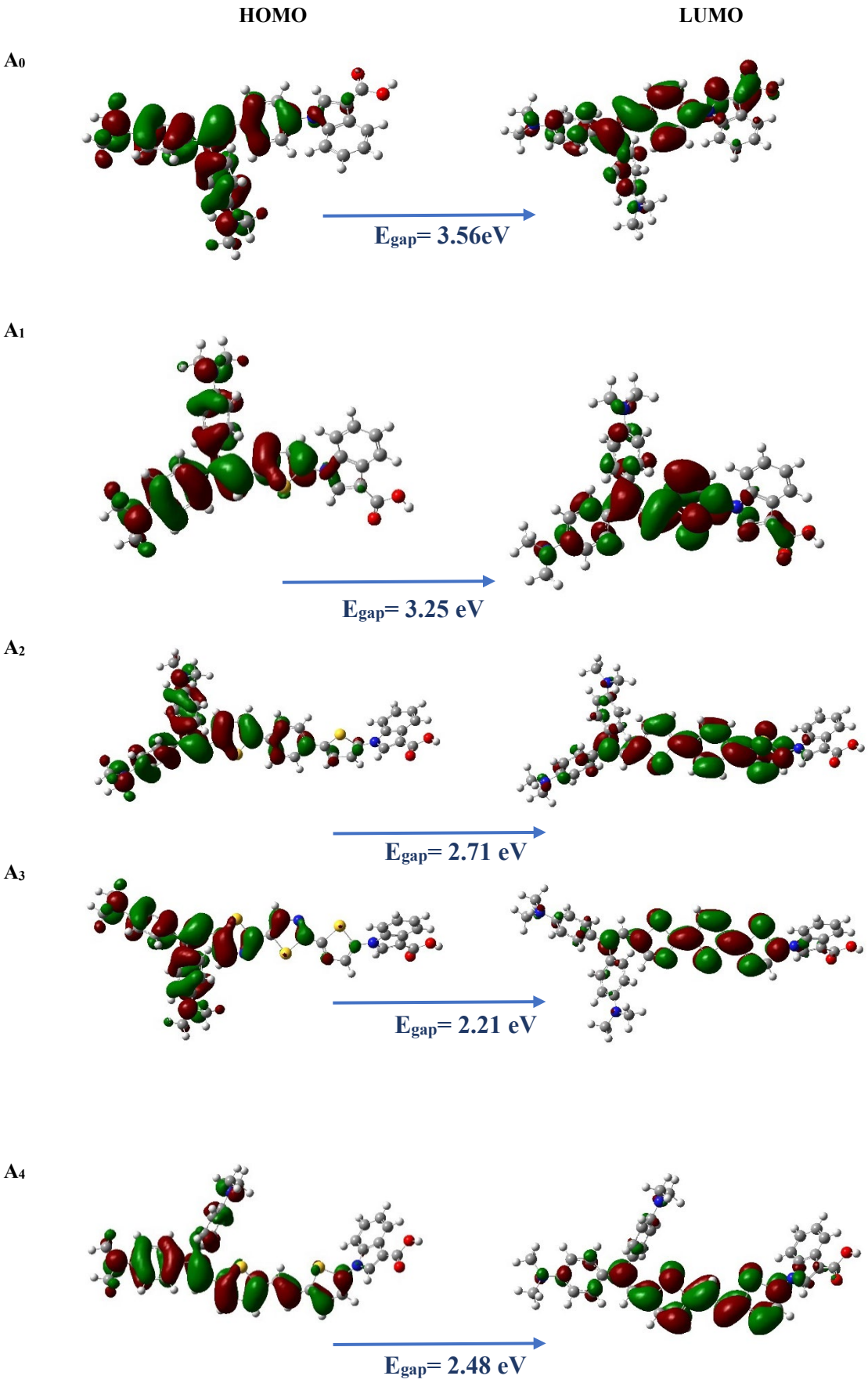

Fig. 5. Contour plots of the FMOs of all dyes examined.

Table. 2. Band gap energy, HOMO, LUMO values of the studied structures

	E_{HOMO} (eV)	E_{LUMO} (eV)	E_{GAP} (eV)
A_0	-5.02	-1.64	3.56
A_1	-5.00	-.175	3.25
A_2	-4.84	-2.13	2.71
A_3	-5.06	-2.85	2.21
A_4	-4.80	-2.32	2.48
TiO_2	****	-4.00	****
I^-/I^{3-}	-4.80	****	****

The results in **Table 2** show that modifications to the π-bridge have a significant impact on the energy gap. Molecule A_3 exhibits the smallest E_{GAP} of 2.21 eV, followed by A_4 (2.48 eV), A_2 (2.71 eV), A_1 (3.25 eV), and A_0 (3.56 eV). The proposed molecules (A_1–A_4) display lower Eg values than A_0, implying that A_1 to A_4 (the new sensitizers) could achieve a higher short-circuit current density (Jsc) than A_0.

4.3 Density of States (DOS):

Numerous studies have demonstrated that density of states (DOS) analysis can elucidate the charge transfer characteristics of organic semiconductors. It also enables the determination of the contributions from various molecular orbitals (MOs) of each component within the molecule to the overall system.[43] The DOS function can be determined using the GaussSum software.

Fig. 6 showcases the DOS analysis, which forecasts the alpha (associated with the valence bands) and beta (associated with the conduction bands) free electrons. The bandgap energy increases in parallel with the DOS of the molecules being studied. In dye-sensitized solar cells (DSSCs), the voltage is influenced by the redox potential of the electrolyte and the energy gap between the Fermi level, located near the conduction band of the TiO_2 semiconductor electrode. In general, when the Fermi energy (EF) is close to the middle of the bandgap, charge is transferred to and from the metal electrode and the organic material. Thus, the energy potential profile remains constant as EF approaches the HOMO or LUMO levels, making the charge transfer significant.[44]

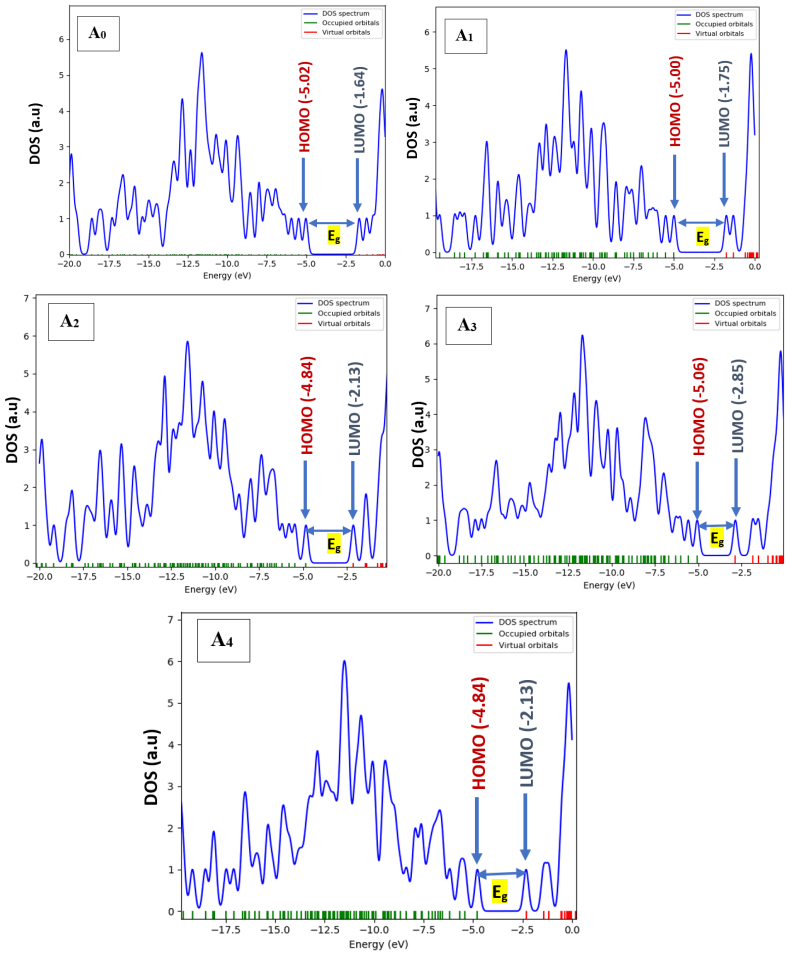

Fig. 6. Density of states for the examined molecules A_0 - A_4

4.4 Quantum Chemical Reactivity Indices

The chemical reactivity indices, including chemical potential (μ), chemical hardness (η), and electronegativity (χ) of the studied molecules, were calculated from the previous equations using the B3LYP method with the 6-311G+(d,p) basis set.[39] The results are presented in **Table 3**.

Table. 3. Calculated values for the electronic and chemical parameters of the four dyes studied

dye	E_{HOMO}(eV)	E_{LUMO} (eV)	E_{GAP} (eV)	μ (eV)	η (eV)	χ (eV)
A_0	-5.02	-1.64	3.56	-3.33	1.69	3.33
A_1	-5.00	-.175	3.25	-3.37	1.62	3.37
A_2	-4.84	-2.13	2.71	-3.48	1.35	3.48
A_3	-5.06	-2.85	2.21	-3.95	1.10	3.95
A_4	-4.80	-2.32	2.48	-3.56	1.24	3.56
TiO_2	****	-4.00	****	-4.66	3.78	4.66

The data show that The TiO_2 compound exhibits the lowest chemical potential at −4.66 eV. compared to the molecules A_0–A_5. This indicates that the transfer of electrons from the dyes, which function as electron donors, to the TiO_2 semiconductor, serving as the electron acceptor, would occur with relative ease.[28] Additionally, The chemical hardness (η) of the molecules examined is lower than that of TiO_2 (η = 3.78 eV), [45] suggesting that these dyes have a greater tendency to release electrons compared to TiO_2. Furthermore, the electronegativity of TiO_2 (−4.66 eV) exceeds that of the dyes, implying that TiO_2 is more capable of accepting electrons from these dyes.

4.5 Natural bond orbital (NBO) analysis

Table 4. NBO analysis for all the proposed molecules (A_0– A_4)

Dyes	D	π	D	A	Δq(D-A)
A_0	0.05655	0.16475	-0.16458	-0.06614	0.12269
A_1	0.07221	0.14331	-0.1574	-0.05811	0.13032
A_2	0.06847	0.14123	-0.15583	-0.05392	0.12239
A_3	0.12093	0.06336	-0.13624	-0.04804	0.16897
A_4	0.08132	0.12551	-0.15117	-0.05567	0.13699

The Natural Bond Orbital (NBO) analysis is a crucial method for examining charge transfer mechanisms and conjugative interactions of molecular systems. It provides significant insights into both intramolecular and intermolecular bonding characteristics. In this study, NBO analysis was performed at the DFT/B3LYP/6-31G level to evaluate the charge distribution within the investigated dyes,[27] as summarized in **Table 4**. The donor (D) and π-linker groups in all molecules exhibited positive NBO charges, confirming their strong electron-donating nature. Conversely, the supplementary acceptor (A) and main acceptor units showed negative NBO values, highlighting their efficiency in withdrawing electrons. Under photoexcitation conditions, the NBO charges on the donor groups followed the trend: A_3 (0.12093e) > A_4 (0.08132e) > A_1 (0.07221e) > A_2 (0.06847e) > A_0 (0.05655e), suggesting that A_3 possesses the highest electron-donating capability. Regarding the acceptor groups, the NBO charges for A_0–A_4 were −0.06614, −0.05811, −0.05392, −0.04804, and −0.05567e, respectively. This pattern indicates that structural modifications in the molecules influence the acceptor's electron-withdrawing efficiency, thereby impacting the overall charge transfer process. Furthermore, the Δq(D–A) parameter represents the extent of charge separation between the donor and acceptor units. As shown in Table 4, the highest charge separation was observed in A_3 (0.16897e), followed by A_4 (0.13699e), A_1 (0.13032e), A_0 (0.12269e), and A_2 (0.12239e). These findings highlight A_3 as the most efficient molecule in terms of charge separation, making it a strong candidate for applications requiring effective charge transfer, such as organic photovoltaics and optoelectronic devices.

4.6 Electrostatic Potential (ESP)

The electron density plays a key role in forecasting the reactivity of electrophilic and nucleophilic sites. (i.e., explaining chemical reactions) as well as hydrogen bonding interactions.[46] The molecular electrostatic potentials (MEP) of the dyes A_0–A_5 are depicted in Figure 7. The red area indicates negative potentials (electron-rich zones), characterizing the reactive sites for electrophilic attacks. Conversely, the blue area represents positive potentials (electron-poor zones), indicating the reactive sites for nucleophilic attacks.

The MEP values reveal that the region of maximum positive potential (in blue) for all dyes is primarily centered on the hydrogen atom of the carboxyl group. Conversely, the region of negative potential (in red) is mainly centered around the oxygen atoms of the acceptor groups (–CO) in dyes A_0–A_5, which constitute the most favorable sites for interaction with the electrolyte.

4.7 Electronic Absorption Spectra:

An effective organic solar cell requires a wide and strong absorption spectrum in the visible range.[47] To examine the impact of various π-spacers in the proposed dyes (A_1–A_5) relative to the reference molecule (A_0), and to gain a deeper

insight into the potential electronic transitions of the four dyes under investigation, the electronic transitions and absorption characteristics were calculated using TD-DFT/B3LYP/6-311G.

The data presented in Table 5 reveal that the maximum absorption wavelengths for the reference molecule (A_0) and its derivatives A_1= 402.13nm, A_2= 420.16nm, A_3= 503.60nm, and A_4 =545.84 nm.

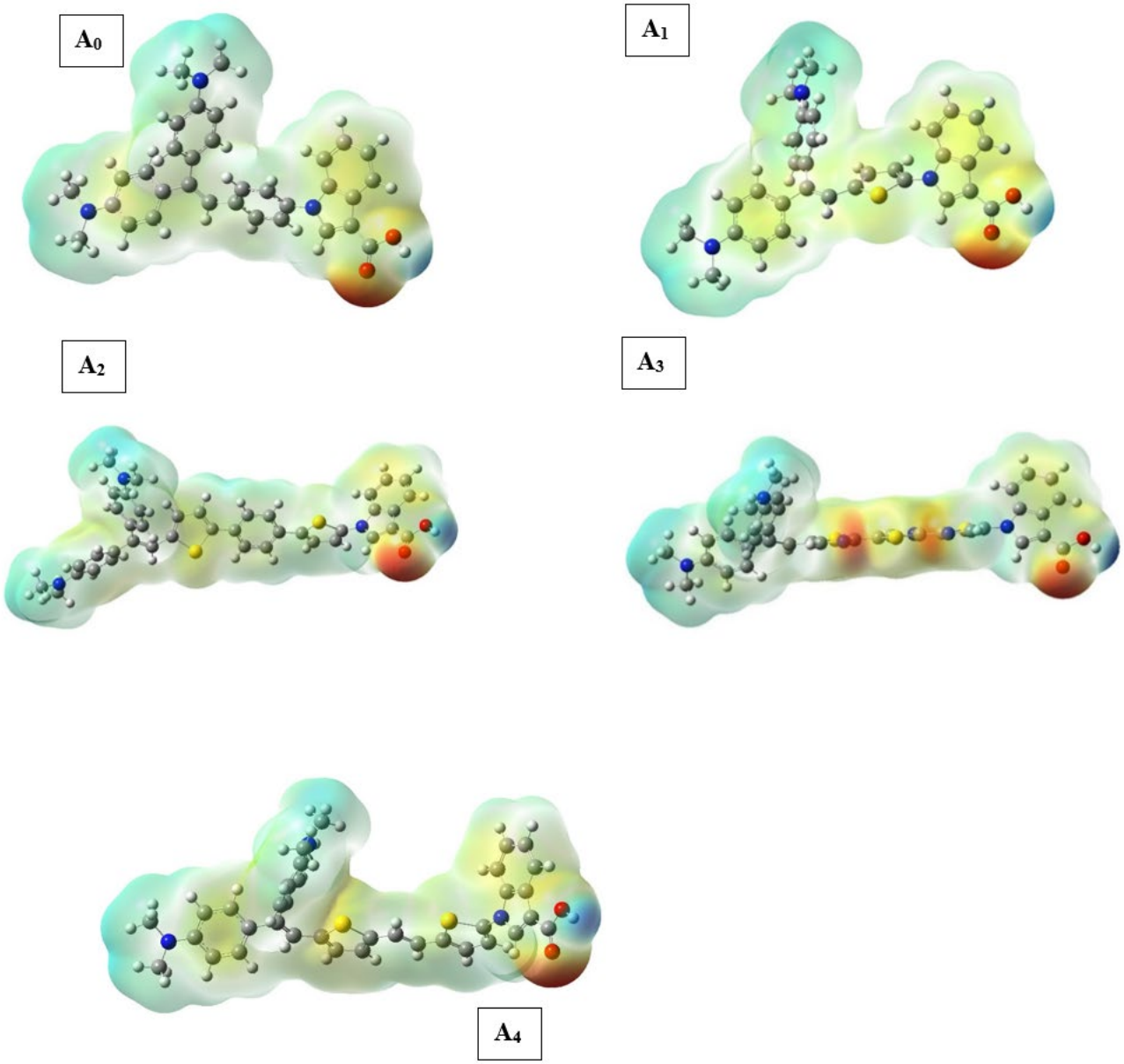

Fig. 7. Calculated electrostatic potentials on the molecular surfaces of the studied dyes.

The proposed dyes showed high absorption in the visible region between 400 and 800 nm. These values correspond to the lowest excitation energy and are attributed to an electronic transition from the ground state S_0 to the excited state S_1.

Additionally, the maximum absorption wavelengths were 627.68 nm for A_3 and 545.84 nm for A_4.
Indeed, a dominant transition with low energy (1.97–3.08 eV) and a higher oscillation strength (0.70–1.18) was observed.

Table 5. Maximum absorption wavelength (λmax), vertical excitation energies (Eex), and oscillator power (*f*) for the investigated dyes

	λ_{max} (nm)	E_{ex} (eV)	*f*
A_0	402.13	3.0832	0.6983
	361.17	3.4328	0.2687
	345.18	3.5919	0.0452
A_1	420.16	2.9509	0.6822
	375.81	3.2991	0.2376
	366.75	3.3806	0.0828
A_2	503.60	2.4620	1.1821
	415.53	2.9837	0.1404
	386.88	3.2047	0.1862
A_3	627.68	1.9753	0.8162
	521.39	2.3779	0.1209
	436.77	2.8386	0.7202
A_4	545.84	2.2714	1.0447
	460.37	2.6932	0.2932
	398.97	3.1076	0.4281

4.8 Parameters Affecting the Photovoltaic Performance of DSSCs

The influence of various π-bridges on the efficiency of dye-sensitized solar cells was determined by studying essential parameters such as ΔG^{inject}, ΔG_{reg}, and LHE. These parameters are essential for evaluating the short-circuit currents (Jsc) and open-circuit voltages (Voc). LHE and ΔG^{inject} play crucial roles in influencing Jsc. Effective dyes must have a high LHE to absorb the majority of photons in the UV-visible region and inject the photoexcited electrons into the conduction band (CB) of TiO_2. Table 6 shows that dyes A_2 and A_4 have the highest LHE values (0.93), followed by A_3 (0.85), and A_0 and A_1 (0.8). This suggests that A_2–A_4 have a superior light absorption potential compared to A0, resulting in higher Jsc values.

Table. 6. Calculated electronic properties of the studied dyes (in eV)

	E_{HOMO}	E_{LUMO}	E_{00}	E^{dyes}	E^{dyes*}	ΔG^{inject}	ΔG_{reg}	LHE	V_{oc}
A_0	-5.02	-1.64	3.08	5.02	1.94	-2.06	0.42	0.80	2.36
A_1	-5.00	-.175	2.95	5.00	2.05	-1.95	0.20	0.79	2.25
A_2	-4.84	-2.13	2.46	4.84	2.24	-1.76	0.04	0.93	1.87
A_3	-5.06	-2.85	1.97	5.06	3.09	-0.91	0.26	0.85	1.15
A_4	-4.80	-2.32	2.27	4.80	2.53	-1.47	0.00	0.90	1.68

Negative values of ΔG^{inject} indicate that electrons can be easily injected into TiO_2. Table 5 also shows that the ΔG^{inject} values for A_2, A_3, and A4 are lower than those for A_0 and A_1, indicating easier electron injection for the former dyes.
For rapid electron transfer, ΔG_{reg} must be as low as possible. Table 5 shows that the ΔG_{reg} values for all the developed dyes are lower than those for A_0, indicating better power conversion efficiency.

5. Conclusion

In this research, we designed and investigated four D–π–D–A sensitizers for dye-sensitized solar cells (DSSCs) to evaluate the impact of different π-bridges on their electronic, optical, and transport properties. We used the TD-DFT/B3LYP/6-311G method to determine the absorption energies, oscillator strengths (f), maximum absorption wavelengths (λmax) and band gaps of these dyes. The results showed that dyes A_2 and A_4 possessed the highest values of light-harvesting efficiency (LHE), suggesting that these dyes could offer superior photovoltaic performance compared to the reference dye A_0. It is also noteworthy that A_1–A_4 exhibited broader absorption bands, indicating a better light absorption capacity. Additionally, the negative ΔG^{inject} values indicate that electrons can be easily injected into TiO_2. Furthermore, the ΔG_{reg} values of the new compounds are lower than those of A_0, suggesting better power conversion efficiency for these dyes.

This study reveals that modifications to the π-bridge units of the reference dye significantly impact the overall performance of the studied dyes. This work should provide theoretical foundations for the development and experimental testing of highly efficient D–π–D–A type sensitizing materials.

References

1 O'Regan B., and Schwartz D. T. (**1998**) Investigation of chemical materials in innovative applications. *Chem. Mater.*, 10(6), 1501.
2 Pretis F., Schwarz M., Tang K., Haustein K., and Allen M. R. (**2018**) Impact analysis of environmental changes. *Philos. Trans. R. Soc. A*, 376, 20160460.
3 Dellink R., Lanzi E., Château J., Bosello F., Parrado R., and de Bruin K. (**2014**) Economic modeling for climate change adaptation. *OECD Econ. Dep. Work. Pap.*, 1135.

4 Tol R. S. J. (**2018**) Critical review of environmental economics policies. *Rev. Environ. Econ. Policy*, 12(1), 4.
5 Newell R. G., Prest B. C., and Sexton S. E. (**2020**) Future resource management strategies. *Washington, DC: Resources for the Future*; (Resour. Future Work Pap. 18-17)..
6 Kakiage K., Aoyama Y., Yano T., Oya K., Fujisawa J., and Hanaya M. (**2020**) Innovations in chemical communications. *Chem. Commun.*
7 Mathew S., Yella A., Gao P., Humphry-Baker R., Curchod B. F. E., Ashari-Astani N., Tavernelli I., Rothlisberger U., Nazeeruddin M. K., and Grätzel M. (**2014**) Advancements in chemical processes. *Nat. Chem.*, 6(3), 242.
8 Ye M., Wen X., Wang M., Iocozzia J., Zhang N., Lin C., and Lin Z. (**2015**) Emerging trends in material sciences. *Mater. Today*, 18(3), 155.
9 Zhang Q., and Liu X. (**2012**) Innovative approaches in nanotechnology. *Small*, 8(24), 3711.
10 Urbani M., Grätzel M., Nazeeruddin M. K., and Torres T. (**2014**) Comprehensive chemical reviews on advanced materials. *Chem. Rev.*, 114(24), 12330.
11 Burke A., Ito S., Snaith H., Bach U., Kwiatkowski J., and Grätzel M. (**2008**) Nanotechnology advancements in solar energy. *Nano Lett.*, 8(4), 978.
12 Wang X., Tang Q., He B., Li R., and Yu L. (**2020**) Recent trends in chemical communications. *Chem. Commun*.
13 Lee T.-H., Hsu C.-Y., Liao Y.-Y., Chou H.-H., Hughes H., and Lin J. T. (**2014**) Advancements in chemical research in Asia. *Chem. Asian J.*
14 Xiang W., Gupta A., Kashif M. K., Duffy N., Bilic A., Evans R. A., Spiccia L., and Bach U. (**2013**) Sustainable chemical processes for energy. *ChemSusChem.*
15 Lee T.-H., Hsu C.-Y., Liao Y.-Y., Chou H.-H., Hughes H., and Lin J. T. (**2014**) New chemical innovations in Asia. *Chem. Asian J.*
16 Lo C.-Y., Kumar D., Chou S.-H., Chen C.-H., Tsai C.-H., Liu S.-H., Chou P.-T., and Wong K.-T. (**2016**) Applied materials in chemical interfaces. *ACS Appl. Mater. Interfaces.*
17 Santhosh K., Ganesan S., and Balamurugan S. (**2021**) Electrochemical advancements in energy storage. *Electrochim. Acta*, 389, 138771.
18 Mehboob M. Y., Riaz Hussain M. A., Saira U. F., Irshad Z., and Janjua M. R. S. A. (**2022**) Innovations in physical chemistry. *J. Phys. Chem. Solids*, 162, 110508.
19 Boutkbout Nait Moudou M., EL Ouafy H., Halil L., Aamor M., Naciri S., Chriyaa M. R., Iken W., and EL Ouafy T. (**2025**) Exploring the role of π-spacers in six novel push-pull photovoltaic systems based on N-methylarylamine: A theoretical DFT investigation. *Comput. Theor. Chem.*, 1244, 115023-115035.
20 Numbury, S. B., Khalfan, M. S., and Vuai, S. A. H. **(2024)** Theoretical studies of electronic and optical characteristics in donor-π-Acceptor (D-π-A) dyes: DFT and TD-DFT methods. *Oxford Open Materials Science*, 4(1), itad022.
21 Preat J., Michaux C., Jacquemin D., and Perpète E. A. (**2009**) Computational studies in chemical physics. *J. Phys. Chem. C*, **113**(39), 16821.
22 Yang Y., Miao X., Liu C., Huang Y., Li L., Zeng L., Li J., Sun H., and Gong M. **(2025)** Charge transfer and photophysical properties of DSSCs based on different π-conjugated bridges: DFT and TD-DFT study. *J. Mol. Graph. Model.*, 137, 108986.
23 Tripathi A., Kumar V., and Chetti P. (**2022**) Photochemical processes and applications. *J. Photochem. Photobiol. A Chem.*, 426, 113738.
24 Iken W., EL Ouafy H., Naciri S., Chriyaa M. R., Halil L., Aamor M., Boutkbout Nait Moudou M., and EL Ouafy T. (**2025**) Effects of van der Waals interactions on the dipole moment and adsorption energy of H_2O on Au(100) and Cu(100) surfaces: Density functional theory study. *J. Indian Chem. Soc.*, 102, 101597.
25 Wang Y., Zhang H., Tang G., and Zhao J. (**2024**) Computational studies in theoretical chemistry. *Comput. Theor. Chem.*, 1236, 114602.
26 Preat J., Michaux C., Jacquemin D., and Perpète E. A. (**2009**) Advances in chemical physics research. *J. Phys. Chem. C*, 113(39), 1682.
27 Kacimi R., Raftani M., Abram T., Azaid A., Ziyat H., Bejjit L., Bennani M. N., and Bouachrine M. **(2021)** Theoretical design of D-π-A system new dyes candidate for DSSC application. *Heliyon*, 7, e07171.
28 Boutkbout Nait Moudou M., EL Ouafy H., Iken W., Chriyaa M. R., Naciri S., Halil L., Aamor M., and EL Ouafy T. **(2025)** Computational DFT Study on Donor and Spacer Substitution in Arylamine-Based Push-Pull Molecules for Enhanced Photovoltaic Performance. *Phys. Chem. Res.*, 13, 197-215.
29 Javed M., Farhat A., Jabeen S., Khera R. A., Khalid M., and Iqbal J. (**2021**) Computational approaches in theoretical chemistry. *Comput. Theor. Chem.*, 1204, 113373.
30 Ouachekradi M., Elkabous M., and Karzazi Y. **(2025)** Triphenylamine-based D-A-π-A dyes for DSSC applications: Theoretical study on the impact of auxiliary acceptor groups and π-bridges on photovoltaic performance using DFT and TD-DFT calculations. *J. Photochem. Photobiol. A: Chem.*, 461, 116152.
31 Adamo C., and Barone V. (**1999**) Contributions to chemical physics theories. *J. Chem. Phys.*, 110(13), 6158.
32 Lakshminarayana B. N., Sreenatha N. R., Sharath C. L., Geetha D. V., Shivakumar N., and Balakrishna K. **(2025)** Synthesis and comparative investigations of DFT/B3LYP, B3PW91, CAM-B3LYP, and HSEH1PBE methods applied to molecular structure, spectroscopic analysis, and electronic properties of a novel hydrazone having triazole and pyrazole moiety. *Results in Chemistry*, 14, 102105.
33 Vuai S. A. H., Khalfan M. S., and Numbury S. B. **(2021)** DFT and TD-DFT studies for optoelectronic properties of

coumarin-based donor-π-acceptor (D-π-A) dyes: applications in dye-sensitized solar cells (DSSCs). *Heliyon*, 7, e08339.
34 Azaid A., Raftani M., Alaqarbeh M., Kacimi R., Abram T., Khaddam Y., Nebbach D., Sbai A., Lakhlifi T., and Bouachrine M. (**2022**) Recent advances in chemical materials. *RSC Adv.*, 12(52), 30626.
35 Afolabi S. O., Semire B., and Idowu M. A. (**2021**) Chemical research findings on molecular interactions. *Heliyon*, 7.
36 Aamor M., EL Ouafy H., Halil L., Boutkbout Nait Moudou M., Chriyaa M. R., Iken W., Naciri S., and EL Ouafy T. (**2024**) Spectroscopic analysis and theoretical comparison of the reactivity of 6-amino-3(R)benzophenone reactions with acetylacetone. *Chem. Rev. Lett.*, **7**, 942-956.
37 Zhao N.-J., Wang Y.-W., Liu Q., Lin Z.-H., Liang R., Fu L.-M., Ai X.-C., Bo Z., and Zhang J.-P. (**2016**) Nanoscale innovations in material science. *Nanoscale.*
38 EL Ouafy H., Aamor M., Oubenali M., Mbarki M., EL Haimouti A., and EL Ouafy T. (**2022**) Theoretical study of the stability and reactivity of salicylic acid isomers by the DFT method. *Curr. Chem. Lett.*, 11, 183-190.
39 Tripathi A., Kumar V., and Chetti P. **(2022)** Impact of internal (donor/acceptor) moieties and π-spacer in triphenylamine-based dyes for DSSCs. *J. Photochem. Photobiol. A: Chem.*, 426, 113738.
40 Singh M., Nadendla S., and Kanaparthi R. K. **(2023)** Unravelling the effect of donor-π-acceptor architecture in designing 1,3-indanedione based sensitizers for DSSC applications. *J. Photochem. Photobiol. A: Chem.*, 435, 114328.
41 Dennler G., Scharber M. C., and Brabec C. J. (**2009**) Breakthroughs in advanced materials. *Adv. Mater.*, **21**(13), 1323.
42 Muñoz-García A. B., Benesperi I., Boschloo G., Concepcion J. J., Delcamp J. H., Gibson E. A., Meyer G. J., Pavone M., Pettersson H., Hagfeldt A., and Freitag M. (2021) Comprehensive review on chemical societies. *Chem. Soc. Rev.*, **50**(22), 12450.
43 Stankevych A., Vakhnin A., Andrienko D., Paterson L., Genoe J., Fishchuk I., Bässler H., Köhler A., and Kadashchuk A. (2021) Applied physics insights in materials. *Phys. Rev. Appl.*, 15, 044050.
44 Kahn A. (**2015**) Emerging horizons in material sciences. *Mater. Horiz.*
45 Zhou Z., and Parr R. G. (**1989**) Insights into chemical interactions. *J. Am. Chem. Soc.*, 111(20), 7371.
46 Raftani M., Abram T., Bennani N., and Bouachrine M. (**2020**) Results in theoretical and chemical research. *Results Chem.*, 2, 100040.
47 Ding W.-L., Wang D.-M., Geng Z.-Y., Zhao X.-L., and Xu W.-B. (2013) Developments in dyes and pigments chemistry. *Dyes Pigments.*